D. F. Kyser
K. Murata

Quantitative Electron Microprobe Analysis of Thin Films on Substrates

Abstract: Monte Carlo simulation procedure is developed for kilovolt electron beam scattering and energy loss in targets consisting of thin films on thick substrates. Such calculations have direct application to the nondestructive quantitative chemical analysis of ultra-thin films in the electron microprobe (an electron probe x-ray microanalyzer), utilizing characteristic x-ray fluorescence. Angular elastic scattering is calculated in the electron trajectory simulation with the screened Rutherford expression for cross section, and energy loss between elastic scattering events is calculated with the continuous-slowing-down approximation of Bethe. The contribution to x-ray fluorescence from the film due to backscattered electrons from the substrate is accounted for.

For elemental films, the Monte Carlo simulation predicts intensity ratios k_i for characteristic x-rays from the film, referenced to standards of thick elemental samples. No film standards are required, and the mass thickness of any elemental film on any substrate can be determined from theoretical calibration curves. The model has been verified by measurements on films of Si, Cu, and Au on Al_2O_3 over wide ranges in E_0 and t. For alloy films, calibration curves are generated and graphically iterated to provide independent analysis of weight fractions C_i and total mass thickness ρt. Films of Mn_xBi_y and Co_xPt_y were successfully analyzed with $\rho t \leq 100 \, \mu g/cm^2$.

Introduction

Quantitative electron microprobe analysis of thin films on thick substrates is a technologically important and challenging problem for which there are two possible solutions. If the film thickness is sufficient to stop the electron beam before penetration into the substrate, then the conventional ZAF model [1] can be utilized to transform the measured x-ray fluorescence intensity into chemical weight fraction. This boundary condition on electron penetration often requires the use of long wavelength x-rays with low excitation threshold energies, for example, L and M series emission lines, with subsequent uncertainties such as the values for absorption coefficients and the absorption correction models. There can also be low sensitivity for measurement of such soft x-rays.

The second approach is to use high electron beam energies and measure short wavelength x-rays with their inherently higher sensitivity and lower absorption correction. However, a correction must then be made for loss of x-ray fluorescence intensity from the film due to electron penetration into the substrate. Previous work on this second approach has been done by Hutchins [2], Colby [3], and Reuter [4] with some success using semiempirical models. Bolon and Lifshin [5] have recently described the application of a simplified Monte Carlo simulation to the thin film problem, and Ballantyne [6] has also utilized a similar Monte Carlo calcula-tion, which was originally developed by Curgenven and Duncumb [7] for application to thick samples. Warner and Coleman [8] extended the original work of Colby, and Bishop, et al. [9] put into graphical form some previous Monte Carlo calculations made for thick samples, but these are applicable only for special film-substrate combinations.

Of the references [2] through [9] on thin film analysis in the electron microprobe, only [3], [6], [8], and [9] treat multicomponent or alloy films. The others, [2], [4], and [5], treat only single-element films, i.e., they determine only the film thickness. Reference [3] requires prior knowledge of film thickness. References [6] and [8] have limited accuracy because of the simple approximations employed, and reference [9] treats only special cases. Hence there is a need for an accurate and general purpose model to deduce both the total film thickness and chemical weight fraction of alloy films on thick substrates from measurements of x-ray fluorescence in the electron microprobe.

The present work utilizes Monte Carlo calculations of kilovolt electron scattering, energy loss, and ionization distribution versus depth to calculate an intensity ratio k, predicted for each characteristic x-ray fluorescence, between a thin film on a known substrate and a thick standard target. This intensity ratio k is conceptually the same as that utilized for electron microprobe analysis of

thick samples and is always referenced to standards of elemental or compound samples, as shown in Fig. 1. No film standards are required. A single-scattering model in the Monte Carlo simulation is used which has been described previously by Murata, et al. [10, 11] for application to thick samples. The model utilizes the Rutherford equation to describe elastic scattering of electrons by the atomic nuclei and the Bethe equation to describe energy loss between elastic scattering events. The mean free path Λ of the electron is used as a variable step length between elastic scattering events. When the electron crosses the boundary between film and substrate, the ionization rate for elements in the film is set equal to zero unless the electron is subsequently backscattered into the film. Scattering and energy loss, characteristic of the substrate, continue as the electron decelerates in the substrate. Typically the trajectories of 1200 individual electrons are calculated for statistical purposes on an IBM System/360, Model 195 computer.

Monte Carlo simulation

• Scattering model

The single-scattering model of Murata, et al. [10, 11] is utilized to calculate the spatial trajectory and energy of each incident high energy electron. Elastic Rutherford scattering of the electron by atomic nuclei is assumed to control the distribution of angular scattering, and the distance along the trajectory between angular scattering events is given by the mean free path

$$\Lambda = 1/n\sigma = A/N_A\rho\sigma,$$

where n is the volume density of atoms (cm^{-3}), σ the total cross section for scattering (cm^2), N_A Avogadro's number (atoms/mole), A the atomic weight (gm/mole), and ρ the mass density (gm/cm^3).

For a mixed-element target composed of i elements, each with weight fraction C_i,

$$(\rho\Lambda)^{-1} = N_A \sum_i (C_i\sigma_i/A_i). \tag{2}$$

Note that the individual contributions to $\rho\Lambda$ are summed inversely, and that this mean free path or step length between scattering events is now expressed in units of mass distance (gm/cm^2) rather than distance (cm). This method has the advantage of requiring no knowledge of the mass density ρ of a compound target. The use of this unit of distance will become apparent later.

The Rutherford equation is used for the differential scattering cross section

$$\sigma_i'(\theta) = \frac{d\sigma_i(\theta)}{d\Omega} = \frac{Z_i(Z_i+1)e^4}{4E^2(1-\cos\theta+2\beta_i)^2}, \tag{3}$$

where Z_i is the atomic number, e the electron charge,

$$k_A = I'_A/I_A \qquad\qquad k_B = I'_B/I_B$$

(a)   (b)
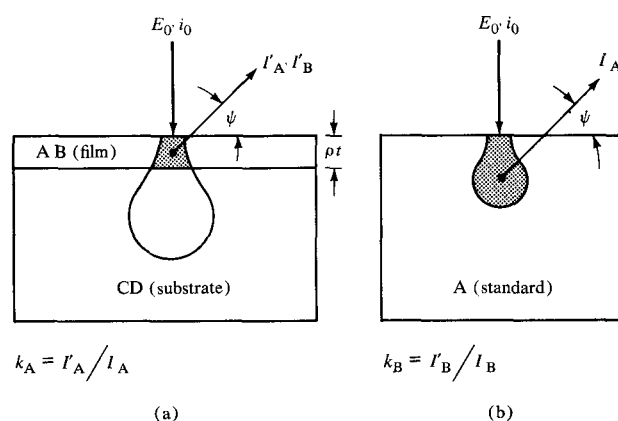
Figure 1 Geometrical configurations of (a) thin film on substrates and (b) standard thick sample, indicating the incident electron beam energy E and the observed line intensity I of x-ray fluorescence. The pear-shaped surface represents the maximum range of primary electrons, and the shaded region is the volume from which x-ray fluorescence is measured.

E the incident electron energy, θ the scattering angle, and β_i the screening parameter to account for electrostatic screening of the nucleus by the orbital electrons [12]. The total cross section σ_i is obtained by integrating Eq. (3) over the range $\theta = 0, \pi$. The probability $P(\theta)d\Omega$ of scattering into the solid angle $d\Omega = \sin\theta\, d\theta d\phi$ is given by

$$P(\theta)d\Omega = (\sigma_i'(\theta)/\sigma_i)d\Omega. \tag{4}$$

If $F(\theta)$ is the indefinite integral of $P(\theta)d\Omega$ over θ, then the directional cosine $(\cos\theta)$ for a particular scattering event can be chosen by means of Monte Carlo techniques by generating a uniformly distributed random number for $F(\theta)$ between 0 and 1. Then $\cos\theta$ is calculated from the relation [10]

$$\cos\theta = 1 - [2\beta F(\theta)/1 + \beta - F(\theta)]. \tag{5}$$

The atom specie i which scatters the incident electron in a mixed target is also chosen in a Monte Carlo fashion by generating another uniformly distributed random number between 0 and 1. The probability that the electron will be scattered by atom i is simply the fractional cross section

$$p_i = (C_i\sigma_i/A_i) \Big/ \sum_i C_i\sigma_i/A_i. \tag{6}$$

Hence if a generated random number R is in the range $(0 - p_i)$, the electron is assumed to be scattered by that specie of atom. If R is in the range $(p_i - 1)$, scattering is caused by another specie of atom. The actual specie of atom that scatters the electron is determined by comparing the generated R with the ranges, 0 to p_1, p_1 to $(p_1 + p_2)$, $(p_1 + p_2)$ to $(p_1 + p_2 + p_3)$, etc. In this manner the atom specie that scatters is determined in a random fashion but is weighted by its fractional cross section.
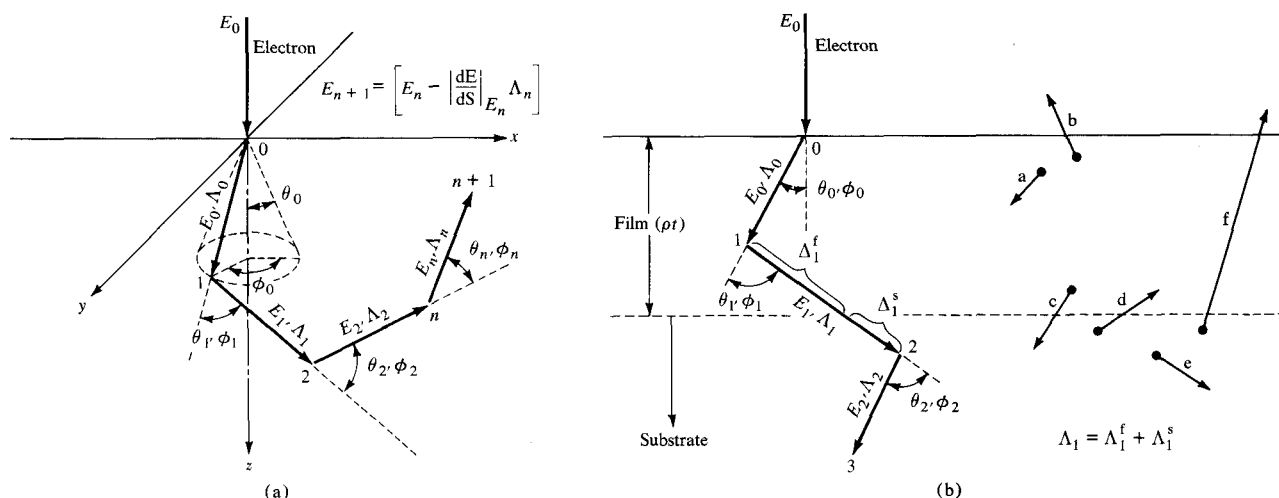
353

Figure 2 Geometry of the initial steps of electron scattering and energy loss (a) in a thick target with a surface at the x-y plane and (b) in a thin film on a thick substrate.

● *Energy loss between scattering events*

The mean energy loss along the trajectory S between elastic scattering events is assumed to be given by the continuous-slowing-down approximation of Bethe,

$$\frac{dE}{dS} = \frac{-2\pi e^4 \rho N_A}{E} \sum_i \left[\frac{C_i Z_i}{A_i} \ln \left(\frac{\gamma E}{J_i} \right) \right], \tag{7}$$

where $\gamma = 1.166$ for relativistic energy electrons and J_i is the mean ionization energy. The numerical values for J_i have been determined experimentally [23] by others from energy loss measurements of energetic particles transmitted through isolated thin films. The mean energy loss is then substituted into Eq. (7) and J_i is calculated, assuming that the Bethe model accurately describes the energy loss. The results of such calculations show that J/Z is approximately constant and is generally between 10 and 15 eV. However, Duncumb and Reed [13] have utilized measurements of x-ray fluorescence from known alloy targets in the electron microprobe to determine values for J/Z, since it enters into the "atomic number" correction of the ZAF model. They find that J/Z is not constant but varies with Z, especially for low values of Z. Fortunately this uncertainty in the numerical value of J_i enters into the Monte Carlo simulation via a logarithm term in Eq. (7), and hence the sensitivity of the final result to this uncertainty is reduced accordingly. However, it still remains as a source of error. The numerical values of J_i used in the present calculations are taken from Duncumb and Reed [13].

● *Sequence in calculation for one trajectory*

The sequence of events in the simulation calculation is shown in Fig. 2(a) for one electron trajectory. An elec-

tron with energy E_0 is impinged at the origin and at 90° to the surface of a semi-infinite target, the x-y plane being the surface. The incident angle can be varied but is normally 90° in modern electron microprobes. The first scattering event is assumed to occur at the origin. The scattering angle θ_0 and step length Λ_0 is calculated by Monte Carlo techniques, as described previously. Since Rutherford scattering is axially symmetric about the incident direction of the electron being scattered, a uniformly generated random number must be used to assign a value to the azimuthal angle ϕ_0. With Λ_0, θ_0, ϕ_0 determined, then the spatial position 1 of the next scattering event is determined with respect to 0. The electron energy at point 1 is then calculated by decrementing the energy with respect to its value at point 0 via Eq. (7). At point 1 the sequence is repeated, using E_1 to calculate θ_1 and Λ_1. Another random number is used to generate ϕ_1, and hence the spatial position of point 2 is found. The sequence is repeated continuously until the electron energy has decreased to some chosen value near to, but greater than, J_i/γ. The sequence is terminated there because Eq. (7) will become indeterminate at lower energies. In addition, the step length becomes very small, and the number of steps increases significantly, as the electron energy decreases. Hence the cutoff energy is also determined by the computer memory size allocated for storage of the numerous variables and data. If the electron escapes the surface as a backscattered electron, the energy and direction is saved in the computer program. In order to represent the averaging effects of a real electron beam that contains many incident electrons, a large number of electron trajectories must be simulated. There will not be any identical

electron trajectories because of the large number of random numbers and step lengths used.

Figure 2(b) shows the sequence of events when the target is composed of a thin film with mass thickness ρt (gm/cm^2) on top of a thick substrate. As the electron traverses the film-substrate boundary, parameters such as Z_i, C_i, Z_i, and J_i must be changed in Eqs. (1-7) to describe the appropriate scattering and energy loss. In addition the various fluxes of electron scattering, as shown by paths a-f in Fig. 2(b), must be accounted for. When the electron crosses a boundary, the scattering and energy loss parameters appropriate to the initial point are used to calculate θ, Λ, and ϕ. However, the parameters appropriate to the terminal point are used in the next calculation.

Figure 3(a) shows 100 simulated electron trajectories for a 20-keV electron beam and 90° incidence on a thick Au target, and Fig. 3(b) for a 1000 Å thin film of Au on a thick Al$_2$O$_3$ substrate. The point beam is incident along the Z axis at $x = y = 0$. The trajectory plots have been projected onto the x-z plane, and hence the y component is not shown. Note that the scales are different by a factor of five, and that the backscattered electron number yield is greater for the thick Au target, as expected. This extreme case of a film material of high atomic number on a substrate material of low atomic number shows dramatically the differences in lateral scattering and depth penetration, compared to that of a homogeneous thick target of high atomic number.

• Ionization rate along electron path

For application to quantitative calculations of characteristic x-ray fluorescence intensity generated and subsequently observed in the electron microprobe, another equation must be introduced to describe the ionization rate for a particular atomic level of atom specie i along the electron path length. The following relation for the ionization cross section $Q_i(E)$ due to Worthington and Tomlin, which was successfully used by Murata, et al. [10, 11] for application to thick targets, is also used here:

$$Q_i(E) = [0.7\pi e^2 / E_{ci}^2 U_i]$$
$$\times \ln [4U_i / 1.65 + 2.35 \exp (1 - U_i)], \qquad (8)$$

where E_{ci} is the critical threshold energy for ionization of a particular level and $U_i = E / E_{ci}$. Along a particular step length dS the electron is assumed to have a constant energy E. Then the number of ions dn_i created of specie i is

$$dn_i = (C_i \rho N_A / A_i) \, Q_i(E) dS. \qquad (9)$$

The number of x-ray photons emitted is then proportional to dn_i, and the contribution from all step lengths is summed, as well as that from all electron trajectories.
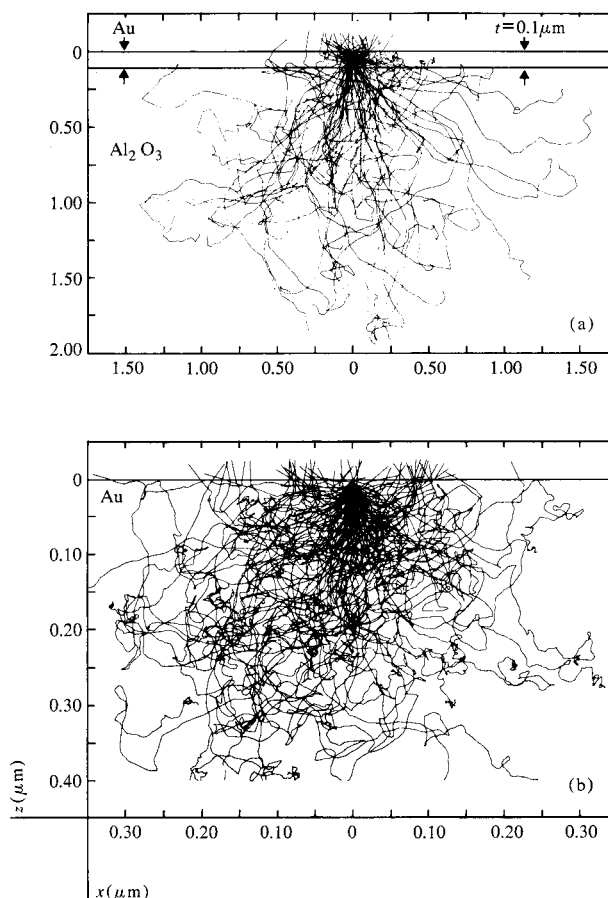
Figure 3 Simulated trajectories of 100 20-keV electrons incident along the z axis for (a) a 1000-Å Au film on Al$_2$O$_3$ and (b) a thick Au target. The trajectories of backscattered electrons are terminated after they emerge from the surface. Note the scale expansion in (b) by 5×.

The numerical factor of proportion (i.e., quantum yield) cancels out in both the experiment and the theory since the intensity is always referenced to that from a standard. The factor $0.7\pi e^2 / E_{ci}^2$ in Eq. (8) cancels out for the same reason. Alternative approximations for $Q_i(E)$, such as that prepared by Reuter [4], were not investigated.

Figure 4 shows the distribution of ionization $\Phi(\rho z)$ with depth ρz calculated for the case of a 20-keV electron beam incident at 90° to a thick Au target and also for a 950 Å thin film of Au on Al$_2$O$_3$. The Au$M\alpha$ characteristic x-ray line ($E_c = 2.24$ keV) was used, and the total intensity generated is given by the integral with depth ρz, i.e., the area under each curve. The k ratio predicted to be measured is the relative value of these areas after correction for internal absorption, which depends on the observation takeoff angle ψ. Note that the distribution of Au$M\alpha$ emission in the film terminates at the film-substrate boundary as it should, and that the shape of the

355
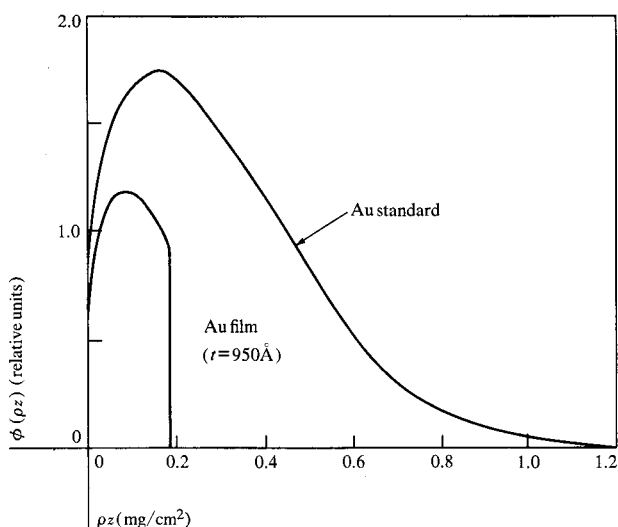
Figure 4 Simulated depth distribution of Au$M\alpha$ fluorescence produced in a Au film on Al$_2$O$_3$ and in a thick Au target by 20-keV electrons.

distribution within the film is significantly different from that in the thick standard. This difference is due to the decreased backscattering from the substrate into the film, and hence displaced peak intensity and more rapid decrease of $\Phi(\rho z)$ with increasing ρz beyond the peak, compared to the thick Au standard. The calculation results shown in Fig. 4 actually originate as a histogram of ionization within finite depth increments, and the data are then smoothly connected.

• *Self-absorption of emerging x-rays*

Since the Monte Carlo simulation calculates the one-dimensional distribution of x-ray *production* with depth ρz, as shown in Fig. 4, a correction for self-absorption of the emerging x-rays must be made before theory and experiment are compared. This correction is accomplished by considering that the fraction f of x-rays generated that escape the target surface at an angle ψ is given by

$$f(\chi) = \int_0^\infty \exp\,(-\chi\rho z)\Phi(\rho z)\,d\rho z \Big/ \int_0^\infty \Phi(\rho z)\,d\rho z, \quad (10)$$

where $\chi = (\mu/\rho)\csc\psi$, and μ/ρ is the mass absorption coefficient for x-rays in target. The observed intensity ratio k_{obs} is then related to the generated intensity ratio k_{gen} by

$$k_{obs} = k_{gen}\,(f\,(\chi)_{sample}/f\,(\chi)_{standard}), \quad (11)$$

where

$$k_{gen} = \frac{\left[\int_0^{\rho t} \Phi(\rho z)\,d\rho z\right]_{sample}}{\left[\int_0^\infty \Phi(\rho z)\,d\rho z\right]_{standard}}, \quad (12)$$

neglecting secondary fluorescence effects. For incremental values of χ, the Monte Carlo computer program also computes $f(\chi)$ for quantitative use with any particular values of (μ/ρ) and ψ.

**Experimental test of the Monte Carlo simulation**

Because we desired to apply the simulation model to quantitative analysis of both the elemental weight fraction and total mass thickness of unknown alloy films on known thick substrates, we first planned to obtain experimental data on the intensity ratio k over a wide range of beam energies E_0 and film thicknesses ρt for single-element films. The next step planned was to obtain the same type of experimental data on multicomponent films. In the latter case two types of binary films were used as experimental samples, as described in the section following.

• *Elemental films*

Initial experimental data were chosen from the work of Reuter [4] for two separate films of Ni on SiO$_2$ and from the work of Bolon and Lifshin [5] for a series of Au films (125 Å-2000 Å) on Si. Except for these Au films on Si, which were measured with $\psi = 18°$, all other experimental measurements to be discussed were obtained in a commercial electron microprobe with $\psi = 52.5°$ and with the electron beam at normal incidence (90°) to the target surface.

Additional films of Si, Cu, and Au on Al$_2$O$_3$ were fabricated in our laboratory by electron beam evaporation from a pure source and by condensation at room temperature onto Al$_2$O$_3$ optical flats. Film thicknesses in the range 125 Å-4000 Å were made. Two films of each thickness were made and one of them used to measure the thickness independently by means of optical interferometry. Because this is a destructive measurement and precludes use of the identical sample for electron microprobe measurements, the companion film was utilized for x-ray data and was assumed to have the same thickness. Large random errors in film thickness would result in discontinuous curves of k vs t, but these were not observed in the measurements to be described. The accuracy of the film thickness measurement by optical interferometry is estimated to be ±50 Å absolute.

Si, Cu, and Au films on Al$_2$O$_3$ were chosen for the following reasons. First, they represent a wide range in atomic number (14, 29, 79) on a substrate of low atomic number and they are easily fabricated. Second, there is no significant secondary fluorescence of Si, Cu, or Au characteristic x-rays by the Al and O characteristic x-rays also produced by electron penetration into the substrate. The simulation model does not account for secondary fluorescence production by line or continuum emission. This effect would generally be small in the film, if
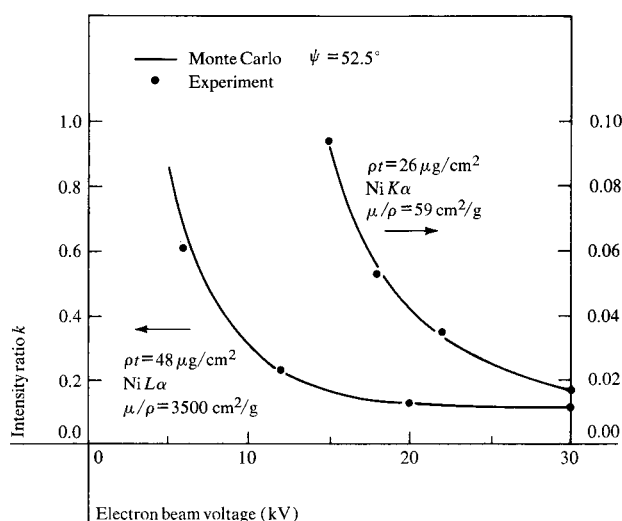
356
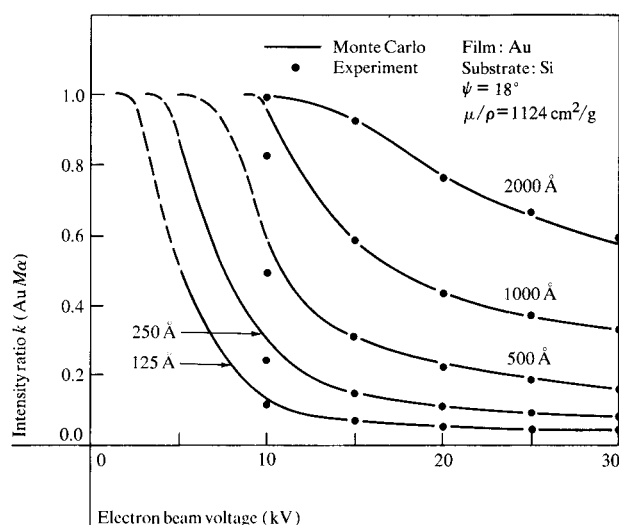
Figure 5 Comparison of Monte Carlo theory with experiment for Au films on Si.

Figure 6 Comparison of Monte Carlo theory with experiment for Ni films on SiO_2.

present at all, but could be significant in the thick standard used for reference. Attempts were made to metallurgically polish a substrate material of high atomic number (W) for deposition of the same elemental films, but a sufficiently smooth surface was not obtained to insure accurate data.

• Binary films

Binary alloys with known chemical composition and in a range of compositions are difficult to fabricate as standard test films. Good results were achieved, however, by utilizing Mn_xBi_y films deposited in a two-source sequential thermal evaporation system with individual rate monitors and controllers in each of the Mn and Bi atom beams directed at the quartz substrate. The ferromagnetic properties of these films were being studied by others in our laboratory. Binary films with approximate Mn *weight* fractions of 0.25, 0.50, and 0.75 were fabricated as well as pure elemental films of Mn and Bi. For the binary films, annealing at 350° C in vacuum after deposition produced homogeneous films. The thickness range for these films was 300 Å-600 Å approximately. No optical interferometry measurements of film thickness were performed.

Another set of Co_xPt_y films on quartz were utilized. These were fabricated by rf sputtering from a cathode source of Co-Pt alloy. The weight fraction of Co in the film was varied systematically by biasing the substrate, thus controlling the relative incorporation rate of Co and Pt in the film during growth. Measurements of the Curie temperature T_c had been made by others in our lab-

oratory who were investigating this material system for its ferromagnetic properties [14]. Comparison of T_c measurements in the film with those made by others on thick standard samples suggested that the films were in the range of 0.10–0.20 weight fraction Co and varied in a systematic manner. The thickness range for these films was 200 Å-600 Å approximately. Again no separate measurements of film thickness were made.

Experimental and theoretical results

• Elemental films

Figure 5 shows the comparison of our Monte Carlo calculations with experimental data for the case of Au films on a Si substrate. The intensity ratio k for the $AuM\alpha$ x-ray has been calculated for a take-off angle of $\psi = 18°$ and then compared with the experimental data of Bolon and Lifshin [5] for 10, 15, 20, 25, and 30 keV and five separate film thicknesses. The dotted portion of the Monte Carlo curves is an approximate extrapolation. No experimental data were obtained there, but the curves must approach a limiting value of $k = 1.0$ at low voltages, and for a vanishingly thin film this limit must occur at $E_c(AuM\alpha) = 2.24$ keV.

Figure 6 shows the comparison of our Monte Carlo calculations with experimental data for the case of two different Ni films on a SiO_2 substrate. The experimental data is that of Reuter [4]. The short-wavelength $NiK\alpha$ fluorescence intensity was measured for the thinner film (26 $\mu g/cm^2$), and the long wavelength $NiL\alpha$ intensity was measured for the thicker film (48 $\mu g/cm^2$). In both

357
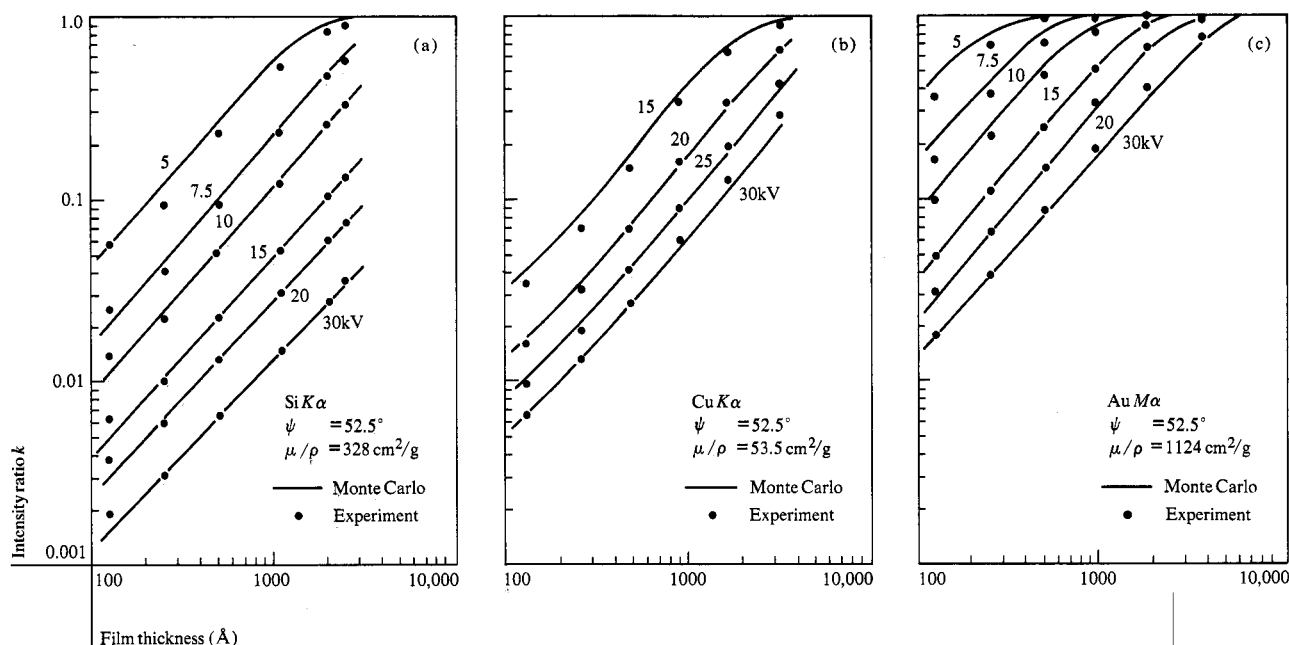
Figure 7 Comparison of Monte Carlo theory with experiment (a) for Si films on Al_2O_3, (b) for Cu films on Al_2O_3, and (c) for Au films on Al_2O_3.

cases an x-ray absorption correction was made with the absorption coefficients (μ/ρ) as indicated and discussed previously.

It has been found necessary to introduce a factor μ into the relation for Λ (Eq. 1) in order to obtain the agreement between theory and experiment shown in Figs. 5 and 6. Thus $\Lambda \propto \mu$ where $\mu = (1 + \alpha)$. The value of α that resulted in the best agreement was determined by comparing the experimental data and Monte Carlo calculations of Figs. 5 and 6, and also by comparing experimental data [15] and Monte Carlo calculations of backscattered electron yield η for thick targets. It appears that the best fit is obtained when an atomic number dependence for μ of the form $(1 + Z/C)$ is used, where C is approximately 300. The primary energy dependence of C has not been established but may be similar to that proposed independently by Bolon and Lifshin [5]. A weak energy dependence may account for the differences between experiment and theory shown in Fig. 5 for low beam voltages. In this and all subsequent calculations, this empirically determined modification to the step length Λ was utilized. The physical justification for using an empirical correction of this magnitude and direction rests mainly upon the assumption that the substitution of Z^2 by $Z(Z + 1)$ in the Rutherford scattering cross section [Eq. (3)] actually overestimates the contribution of electron-electron scattering. Berger [16] has discussed a small correction to the Rutherford single-scattering cross section, due to Spencer, of the form $[1 + g(Z)]$. The qualitative and quantitative effect of that small correction is in reasonable agreement with the effect of the correction factor μ on Λ proposed here. The factor μ may incorporate additional sources of error in the Monte Carlo model, such as the expression for ionization cross section $Q_i(E)$ in Eq. (8).

Figures 7 (a), (b), and (c) show the comparison of Monte Carlo calculations with experiment for the case of Si, Cu, and Au films on Al_2O_3 substrates.

• *Binary films*

The experimental data obtained at 20 keV for the three binary films of $Mn_x Bi_y$ and the two elemental films are listed in Table 1. Data were obtained on three separate x-ray lines: $MnK\alpha$ ($E_c = 6.54$ keV), $BiM\alpha$ ($E_c = 2.60$ keV), and $BiL\alpha$ ($E_c = 13.42$ keV). Also shown in Table 1 is the standard counting error for each calculation of k based on the statistical properties of x-ray emission [17]. This calculation involves the x-ray intensities recorded for the x-ray line and background settings of the spectrometer for both the film-substrate target and the thick standard target. The largest counting error was obtained for the $BiL\alpha$ measurement on the film (X115-7) with the smallest fraction of Bi. This degree of error was due to the extremely low ratios of line to background and the low line intensities encountered. However, the measurement of the $BiL\alpha$ line was redundant

Table 1 Experimental k values obtained from Mn-Bi films on SiO_2 at 20 keV.

Sample	$k(MnK\alpha)$	$k(BiM\alpha)$	$k(BiL\alpha)$
X115-1	——	0.0766	0.109
	——	(0.85)	(1.21)
X115-3	0.0226	0.0515	0.0771
	(0.68)	(0.84)	(1.21)
X115-5	0.0293	0.0220	0.0323
	(0.60)	(1.31)	(2.06)
X115-7	0.0329	0.00668	0.00990
	(0.56)	(2.54)	(2.74)
X115-9	0.0610	——	——
	(0.46)	——	——

(n) = Standard counting error in k (% relative)

Table 2 Experimental k values obtained from Co-Pt films on SiO_2 at 20 keV.

| Sample	$k(CoK\alpha)$	$k(PtM\alpha)$
10-2	0.0177	0.0581
11-2	0.0305	0.114
12-2	0.0148	0.0675
13-2	0.00670	0.0465

and actually undesirable, as described in the next section. Note the extremely low values of intensity ratio k.

The experimental data obtained at 20 keV for the four binary films of Co_xPt_y are listed in Table 2. Data were obtained on two x-ray lines: $CoK\alpha$ ($E_c = 7.71$ keV) and $PtM\alpha$ ($E_c = 2.15$ keV). The standard counting errors were similar to those calculated for the Mn_xBi_y films.

• *Analysis of binary films*

To convert the experimental data of Tables 1 and 2 into values of elemental weight fraction C_i and total film mass thickness ρt, the Monte Carlo computer program for simulation of electron scattering and energy loss is utilized to generate calibration curves of k_i versus C_i, with ρt as a parameter. The Monte Carlo program is not arranged to iterate the matrix effects and converge to a unique solution in the same manner as the ZAF model for thick targets [1], and hence it must be used to generate numerical points on a calibration curve for a particular set of experimental conditions. The results of such calculations are shown in Fig. 8 for the case of Mn_xBi_y films on a SiO_2 substrate at $E_0 = 20$ keV and $\psi = 52.5°$. Calculations of $k(MnK\alpha)$ and $k(BiM\alpha)$ have been made for particular combinations of C_{Mn}, $C_{Bi} = (1 - C_{Mn})$, and
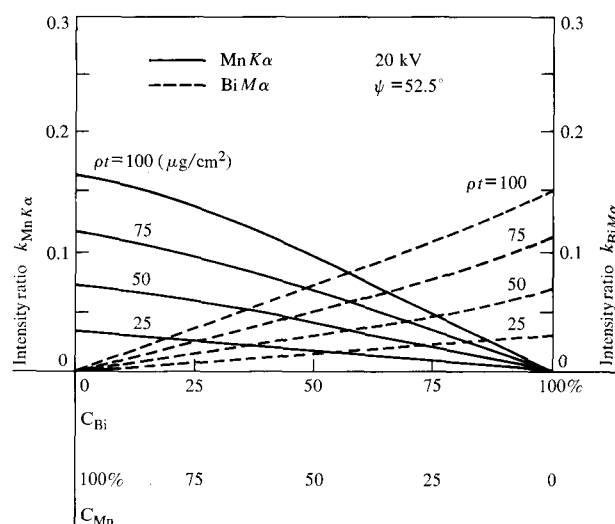
Figure 8 Theoretical calibration curves for Mn and Bi x-ray fluorescence from thin films on SiO_2.

ρt. A smooth line has then been drawn through those points with common values of ρt. Note that the curves are nonlinear with C_i, which is expected because of the difference in scattering and energy loss properties of Mn and Bi atoms. The analysis of the data in Table 1 then reduces to graphical iteration and interpolation of $k(MnK\alpha)$ and $k(BiM\alpha)$ experimentally measured for each film within the calibration curves of Fig. 8 to arrive at a unique fit for both C_i and ρt. This is possible because there are two unknowns (ρt and C_{Mn} or C_{Bi}) and two knowns (k_{Mn}, k_{Bi}).

Graphical convergence is easily accomplished by replotting the calibration curves of Fig. 8 as shown in Fig. 9. The parameters have been interchanged, and calibration curves of $k(MnK\alpha)$ and $k(BiM\alpha)$ have been plotted versus ρt for particular values of C_i. The experimental intensity ratios for each film (e.g., X115-3) are then compared with Fig. 9, and the intercept points provide two separate values for ρt. The object is to find a particular value of C_{Mn} for which these two values of ρt coincide. A unique solution is obtained by plotting $\Delta \rho t$ versus C_i and locating the intercept where $\Delta \rho t = 0$, as shown in Fig. 10. For this particular film (X115-3), the result is $\rho t_0 = 53$ $\mu g/cm^2$ and $C_{Mn} = 0.255$, $C_{Bi} = (1 - C_{Mn}) = 0.745$. The results obtained in this manner for all of the Mn_xBi_y films are shown in Table 3. Also shown in Table 3 are analytical results obtained by nuclear backscattering energy analysis [18], which is the only other nondestructive and quantitative analysis technique known to the authors for alloy films in this thickness range that does not require film standards.

Calibration curves for the $BiL\alpha$ x-ray line were also generated with the Monte Carlo program and compared

359

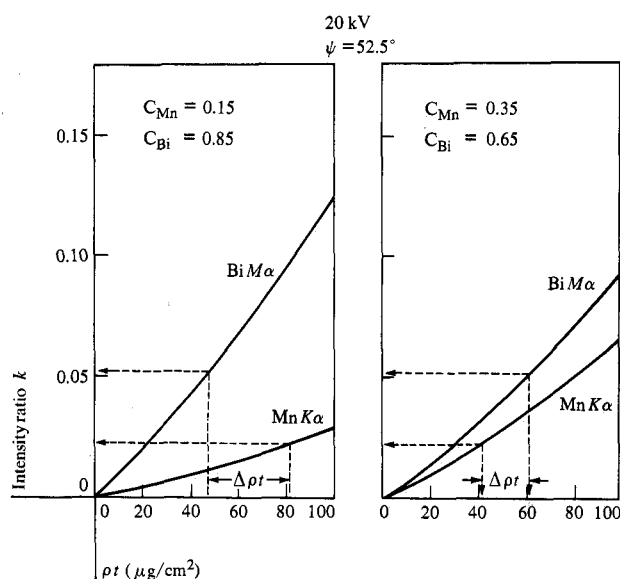**Figure 9** Theoretical calibration curves for Mn and Bi x-ray fluorescence obtained from Figure 8 for two particular values of composition.
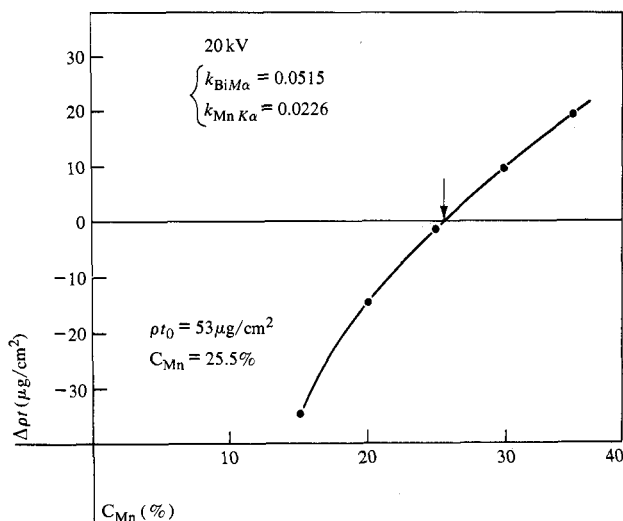

Figure 10 Graphical convergence of experimental data from MnBi film X115-3 within calibration curves of Figure 8.

with experimental values. However, a relatively large correction is required for secondary excitation of the Bi$L\alpha$ line because of continuum radiation generated in the thick Bi standard sample. The correction should be negligible for the thin film on a substrate of low atomic number. Such a correction is also negligible for the longer wavelength Bi$M\alpha$ and Mn$K\alpha$ radiation. This type of correction is not made in the Monte Carlo program and hence must be made with other models. Approximate

calculations of this correction to the Bi standard were made with the model of Springer [19], and then calculations of k(Bi$L\alpha$) compared with experiment. These calculations gave results comparable to those listed in Table 3, within the approximations used. Because of the uncertainties in this correction, and the redundant nature of the measurement, such results were not relied upon for analysis. The results obtained with the Bi$L\alpha$ line, however, were consistent with those obtained with the Bi$M\alpha$ line.

Calibration curves similar to Fig. 8 were also generated for Co$_x$Pt$_y$ films on a SiO$_2$ substrate for the Co$K\alpha$ and Pt$M\alpha$ x-ray lines at $E_0 = 20$ keV, $\psi = 52.5°$. These calibration curves are shown in Fig. 11. Analysis of the experimental data in Table 2 was performed in the same manner as for the Mn$_x$Bi$_y$ films, and the results are listed in Table 4. Also shown in Table 4 are the analytical results obtained for two of the four films by nuclear backscattering energy analysis [18].

Discussion

The Monte Carlo simulation of kilovolt electron beam scattering and energy loss described in this paper appears to accurately predict the intensity ratio k for a wide range of atomic numbers, film thicknesses, and beam energies, as shown in Figs. 5-7. The accuracy is best in general for regions of high beam energy and/or small film thickness. This behavior may be related to the use of the Born approximation inherent in Eq. (7), which treats the Coulomb scattering of electrons by bound electrons as a perturbation [20]. The Bethe expression for energy loss is expected to be more accurate at high energies and low Z because of the Born approximation.

The justification for utilizing the screened-nucleus Rutherford model to describe electron scattering in the keV range is verified in this particular application by the agreement obtained between experiment and theory. Inelastic electron-electron scattering is treated by replacing Z^2 by $Z(Z + 1)$ in the usual manner [21]. As described previously, the correction factor μ to Λ was found necessary in order to obtain this agreement and is thought to be necessary, because the contribution of electron-electron scattering is overestimated in the above approximation.

It has also been suggested [22] that this empirical correction is necessary because of the additional x-ray fluorescence generated by high-energy secondary electrons, or δ-rays [23]. The effect of such secondary electrons on x-ray production is neglected in the present Monte Carlo simulation because the Bethe continuous-slowing-down approximation is used for energy loss.

The Rutherford model, like the Bethe model, is also expected to be more accurate at high energies and low
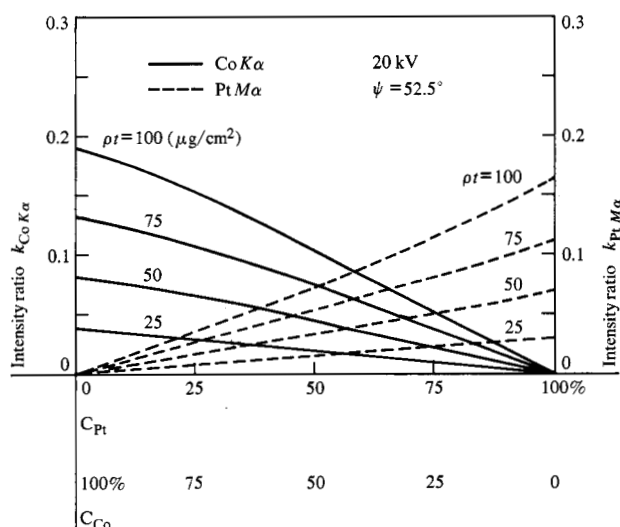
Figure 11 Theoretical calibration curves for Co and Pt x-ray fluorescence from thin films on SiO_2.

Table 3 Monte Carlo and nuclear backscattering analysis results for Mn-Bi films.

Sample	Monte Carlo		Nuclear backscatter	
	$C_{Mn}(\%)$	$\rho t(\mu g/cm^2)$	$C_{Mn}(\%)$	$\rho t(\mu g/cm^2)$
X115-1	0.0	54	0.0	48.6
X115-3	25.5	53	26.6	48.2
X115-5	51.0	38	53.5	33.6
X115-7	80.0	29	80.1	26.2
X115-9	100.0	42	100.0	40.1

Table 4 Monte Carlo and nuclear backscattering analysis results for Co-Pt films.

Sample	Monte Carlo		Nuclear backscatter	
	$C_{Co}(\%)$	$\rho t(\mu g/cm^2)$	$C_{Co}(\%)$	$\rho t(\mu g/cm^2)$
10-2	18.5	53	19.4	49.0
11-2	16.3	89	——	——
12-2	14.0	56	——	——
13-2	10.1	40	9.6	33.6

Z, although the expression for the screening parameter β_i alone is expected to be more accurate at high Z [12, 16]. Fortunately the effect of uncertainties in β_i on angular scattering is small since $\beta_i \ll 1$ in Eq. (3).

The quantitative agreement obtained in Figs. 5-7 for elemental films is also based on the use of bulk mass densities ρ to describe the mass density in thin film form. The use of bulk ρ values may introduce a systematic error into calculations of thickness t when calibration curves such as Figs. 5–7 are utilized to measure unknown films. However, if the real mass density ρ of the film is known and is different from that used in these calculations, then this simply results in a shift of the thickness scale because ρ and t always enter into the Monte Carlo calculations as a linear product ρt. For the alloy films, good agreement on weight fraction C_i is obtained between the Monte Carlo analysis with x-ray fluorescence in the electron microprobe and the nuclear backscattering energy analysis. However, the mass thickness ρt calculated from the latter measurements is systematically less than that obtained from the Monte Carlo analysis. The source of this discrepancy is not known at the present time.

The experimental and theoretical results shown in Fig. 7, where log k is plotted versus log t and E_0 is the parameter, indicate that k is not linear with t over the whole range of t investigated (125 Å- 4000 Å). Experimental measurements of absolute line intensity I' versus t do show a linear dependence on t for $t \leq 300$ Å [24]. Such measurements, however, require a standard reference film of known thickness for calibration of each elemental film, and application to alloy films is expected to change this linear dependence to a nonlinear one. The results described in the present work apply to the measurement of intensity ratio k, not to absolute intensity I, since the former can be done for general application with thick standards. Of course the Monte Carlo simulation does calculate I'_{film} and $I_{standard}$ separately, but the ratio k is the more useful result for quantitative analysis of unknown films.

For application of this Monte Carlo simulation to alloy films with more than two atomic components, the use of calibration curves described in the previous section will be difficult. This is so because each component requires a separate k axis, and graphical iteration will be necessary over a curved surface for the case of a ternary film, as an example. For a ternary film, calibration curves could be generated, assuming a given atomic ratio N between two of the three species, to change the problem into a pseudobinary one. However, N then becomes a variable parameter if it is not known from stoichiometry. A more general approach would be to generate calibration binary curves for all the possible binary combinations of Z in the film and then fit an empirical expression to these binary curves with the a-factor approach of Ziebold and Ogilvie [25]. These a-factors for binary systems could then be utilized as described there for ternary or higher order systems in an iterating and converging computer program such as that described by Bence and Albee [26] or others by Beaman and Isasi [27]. The Monte Carlo simulation described

in the present work is not limited in principle to the number of atomic species in the target for generation of calibration curves. The Monte Carlo simulation is also capable of being applied to quantitative analysis of multiple-layer thin films on a substrate, but the practical use of such an approach is beyond the scope of this paper.

The present simulation can also be directly applied to quantitative analysis of free-standing thin films without a substrate, such as those encountered in transmission electron microscopy. This kind of analysis is easily accomplished by elimination of backscattered electrons from the substrate. The Monte Carlo model should then provide similar accuracy to those proposed by Tixier and Philibert [28] or Hall and Hohling [29] in such cases.

Another application of this particular Monte Carlo simulation that is being pursued by us is the calculation of three-dimensional energy loss contours in polymer films on a metallic substrate, which is of interest in electron beam lithography [30]. We have calculated spatial contours of equi-energy volume density deposited by an electron beam incident on thin polymer films having a Si substrate. These contours are observed by scanning electron microscopy after chemical development of that volume in the film that has absorbed more energy/volume than some critical value. Simulation of the optimum spatial resolution and the effects of substrate backscattering is possible with this model. The results of this work will be published elsewhere [31].

Summary

Monte Carlo simulation of kilovolt electron beam scattering and energy loss has been developed and experimentally verified for targets consisting of thin films on a thick substrate. For elemental films, calibration curves of x-ray line fluorescence intensity ratio with film thickness were generated and verified experimentally over wide ranges in beam energy (5-30 keV), atomic number of the film (14, 28, 29, 79) on low-Z substrates (Si, SiO_2, Al_2O_3), film thickness (125 Å-4000 Å), and x-ray lines ($SiK\alpha$, $NiK\alpha$, $NiL\alpha$, $CuK\alpha$, $AuM\alpha$) appropriate to each configuration. For alloy films, calibration curves of intensity ratio k_i versus weight fraction C_i for the Mn_xBi_y system and the Co_xPt_y system were generated, with total mass thickness ρt as a parameter. These calibration curves were graphically iterated with experimental data from semistandard films to provide a unique analysis of both the weight fraction and mass thickness below 100 $\mu g/cm^2$. These unique analyses correlated with that expected from the manner in which the films were fabricated, as well as with analyses obtained from nuclear backscattering and Curie temperature measurements. The Monte Carlo simulation can be applied to unknown films with intensities that are experimentally referenced

to thick targets, and does not require thin standard films for reference. This technique provides a general model for quantitative and nondestructive chemical analysis of ultrathin films on thick substrates, while retaining the high lateral spatial resolution afforded by the electron probe x-ray microanalyzer.

• Note added in proof

A recent paper by Oda and Nakajima [32] describes a semiempirical method for the simultaneous determination of thin film composition and thickness. The method involves solution of a set of simultaneous equations and includes the effect of backscattered electrons from the substrate. The method appears to be similar to that of [3] and [8] except that no knowledge of film thickness is required. Additional work on the analysis of thin *foils* is described in a section on analytical electron microscopy [33] for application to transmission electron microscope samples, but utilizing thick reference standards. While such techniques have been utilized for quantitative analysis of *foils* [34, 35], they cannot be expected to succeed for thin films on *substrates* because of neglect of the backscattered electrons from the substrate.

References

1. D. R. Beaman and J. A. Isasi, ASTM Special Technical Publication No. 506, 1972.
2. G. A. Hutchins, *The Electron Microprobe*, T. D. McKinley, K. F. J. Heinrich, and D. B. Wittry, eds., John Wiley and Sons Inc., New York, 1966, p. 390.
3. J. W. Colby, *Advances in X-ray Analysis*, Plenum Press, New York, 1968, vol. 11, p. 287.
4. W. Reuter, *Proceedings of the Sixth International Conference on X-ray Optics and Microanalysis*, ed. by G. Shinoda, K. Kohra, and T. Ichinokawa, University of Tokyo Press, Tokyo, 1972, p. 121.
5. R. B. Bolon and E. Lifshin, *Proceedings of the Sixth Annual SEM Symposium*, ed. by O Johari and I. Corvin (IIT Research Institute, 1973), p. 385.
6. J. P. Ballantyne, Ph.D. Thesis, Cambridge University, 1972, Ch. 6 (unpublished).

7. L. Curgenven and P. Duncumb, Tube Investments Research Laboratories Report No. 303, 1971.
8. R. R. Warner and J. R. Coleman, *Micron* 4, 61 (1973).
9. H. E. Bishop and D. M. Poole, *J. Phys. D.* 6, 1142 (1973).
10. K. Murata, T. Matsukawa, and R. Shimizu, *Jap. J. Appl. Phys.* 10, 678 (1971).
11. K. Murata, T. Matsukawa, and R. Shimizu, *Proceedings of the Sixth International Conference on X-ray Optics and Microanalysis*, ed. by G. Shinoda, K. Kohra, and T. Ichinokawa, University of Tokyo-Press, Tokyo, 1972, p. 105.
12. G. Shinoda, K. Murata and R. Shimizu, *Quantitative Electron Probe Microanalysis*, K. F. J. Heinrich, ed., NBS Special Publication No. 298, 1968, p. 155.
13. *Ibid.*, P. Duncumb and S. J. B. Reed, p. 133.
14. D. Treves, J. T. Jacobs, and E. Sawatzky, paper 6D-6, presented at 19th Conference on Magnetism and Magnetic Materials, Boston, 1973 (to be published).
15. H. E. Bishop, *Proceedings of the Fourth International Conference on X-ray Optics and Microanalysis*, ed. by R. Castaing, P. Deschamps, and J. Philibert; Hermann, Paris, 1966, p. 153.
16. M. J. Berger, *Methods in Computational Physics*, ed. by B. Adler, S. Fernbach, and M. Rotenberg, Academic Press, New York, 1963, p. 135, Appendix B.
17. H. A. Liebhafsky, H. G. Pfeiffer, E. H. Winslow, and P. D. Zemany, *X-ray Absorption and Emission in Analytical Chemistry*, John Wiley and Sons, Inc., New York, 1960, Ch. 10, Eq. (10-15).
18. M. A. Nicolet, J. Mayer, and I. Mitchell, *Science* 177, 844 (1972).
19. G. Springer, *Proceedings of the Sixth International Conference on X-ray Optics and Microanalysis*, ed. by G. Shinoda, K. Kohra, and T. Ichinokawa, Univ. of Tokyo Press, Tokyo 1972, p. 141.
20. R. D. Evans, *The Atomic Nucleus*, McGraw-Hill Book Co., Inc., New York, 1955, Appendix C.6.
21. *Ibid.*, Ch. 19.2.
22. P. Sigmund, private communication.
23. H. A. Bethe and J. Ashkin, *Experimental Nuclear Physics*, E. Segré, ed., John Wiley and Sons, Inc., New York, 1953, vol. 1, p. 166.
24. R. Butz and H. Wagner, *Surface Science* 34, 693 (1973).
25. T. O. Ziebold and R. E. Ogilvie, *Anal. Chem.* 36, 322 (1964).
26. A. E. Bence and A. L. Albee, *J. Geol.* 76, 382 (1968).
27. D. R. Beaman and J. A. Isasi, *Anal. Chem.* 42, 1540 (1970).
28. R. Tixier and J. Philibert, *Proceedings of the Fifth International Conference on X-ray Optics and Microanalysis*, ed. by G. Mollenstedt and K. Gaukler, Springer-Verlag, Berlin, 1969, p. 180.
29. *Ibid.*, T. Hall and H. Hohling, p. 582. (See also Ref. 12, p. 269.)
30. E. D. Wolf, F. S. Ozdemir, W. E. Perkins, and P. J. Coane, *Record of the Eleventh Symposium on Electron, Ion, and Laser Beam Technology*, ed. by R. F. M. Thornley, San Francisco Press, 1971, p. 331.
31. D. F. Kyser and K. Murata, Sixth International Conference on Electron and Ion Beams in Science and Technology, San Francisco, May 12-17, 1974.
32. Y. Oda and K. Nakajima, *Nippon Kinzoku Gakkaishi* (*J. Japan Inst. Metals*) 37, 673 (1973). (In Japanese).
33. *Proc. 5th European Congress on Electron Microscopy*, Institute of Physics, London (1972), p. 135.
34. G. W. Lorimer, N. A. Razik and G. Cliff. J. *Microscopy* 99, 153 (1973).
35. M. H. Jacobs, *J. Microscopy* 99, 165 (1973).

D. F. Kyser is located at the IBM Research Laboratory, Monterey and Cottle Roads, San Jose, California 95193; K. Murata is located at the Applied Physics Department, Osaka University, Osaka, 565 Japan.

363